energies

MDPI

Article

Selective Immobilization of Antimony Using Brucite-rich Precipitate Produced during In Situ Hypochlorous Acid Formation through Seawater Electrolysis in a Nuclear Power Plant

Kyung-Hee Lee [1], Yong-Gu Lee [2], Jaegwan Shin [2], Kangmin Chon [2,*] and Sang-Ho Lee [1,*]

[1] Korea Hydro & Nuclear Power (KHNP) Central Research Institute, 70, 1312-gil, Yuseong-daero, Yuseong-gu, Daejeon 34101, Korea; kyunghee.lee@khnp.co.kr

[2] Department of Environmental Engineering, College of Engineering, Kangwon National University, Kangwondaehak-gil 1, Chuncheon-si, Gangwon-do 24341, Korea; yonggulee79@gmail.com (Y.-G.L.); jgshin13@gmail.com (J.S.)

* Correspondence: kmchon@kangwon.ac.kr (K.C.); sangholee3395@gmail.com (S.-H.L.); Tel.: +82-33-250-6352 (K.C.); +82-42-870-5573 (S.-H.L.)

Received: 30 June 2020; Accepted: 26 August 2020; Published: 31 August 2020

Abstract: This study has investigated the selective immobilization of antimony using the brucite (magnesium hydroxide)-rich precipitate (BP) collected from a hypochlorous storage tank in a nuclear power plant of South Korea. The energy dispersive X-ray and X-ray diffraction analyses revealed that the BP mainly consisted of magnesium (72.5%) and its dominant mineral phase was brucite ($Mg(OH)_2$). Therefore, brandholzite ($Mg[Sb(OH)_6]_2 \cdot 6H_2O$) was newly formed through the surface-induced precipitation during the adsorption of antimony using the BP. The adsorbed amount of antimony increased with decreasing pH values because of the increased positive surface charge of the BP (pH_{pzc} = 9.6). The maximum adsorption capacity (Q_{max}) of BP, calculated by Langmuir adsorption isotherm, was 11.02 mg/g. The presence of competitive anions did not significantly affect the adsorption of antimony toward the BP due to its high selectivity. These results suggest that the facile utilization of the BP as a low-cost adsorbent seems to be a practical option for the selective removal of antimony from wastewater.

Keywords: antimony; brucite; brandholzite-like structure; adsorption

1. Introduction

Antimony (Sb) has been known as a toxic substance since it can pose acute and chronic toxicity to living organisms [1–3]. Therefore, the U.S. Environmental Protection Agency (USEPA) established a maximum contamination level of antimony in drinking water of 6 μg/L, established by the U.S. Environmental Protection Agency (USEPA) due to its high toxicity to humans [4]. In the aquatic environment, antimony predominantly exists in inorganic forms, including trivalent and pentavalent chemical species [2,3]. Furthermore, the pentavalent form of antimony was found to be the dominant species under aerobic conditions in groundwater and stream water [3]. The adsorption techniques have been widely applied to remediate water contaminated by antimony because of their cost-effectiveness and high quality effluents [5–7]. Therefore, various types of iron-based and/or aluminum-based adsorbents have been developed to immobilize antimony in drinking and wastewater [8]. In general, iron and aluminum are known to be useful for removing antimony in water due to their high reactivity and adsorption capacity with antimony [7,9,10]. However, their removal of antimony in surface water and/or wastewater can be significantly interfered with by other anions such as arsenic, phosphate,

and chromate due to relative low charge density and large ionic radii. Based on these reasons, numerous researchers have attempted to immobilize antimony with magnesium-based materials through new mineral formation since they exhibit high selectivity for antimony [5,10–12].

Brucite is a mineral form of magnesium hydroxide ($Mg(OH)_2$) and the crystal structure of brucite is comprised of Mg^{2+} cations and OH^- anions arranged in layers of its trigonal structure (space group symmetry: *P3m1*) [13]. In the structure of brucite, the crystal structure consists of edge-sharing MgO_6 polyhedra and each layer is weakly bonded by OH groups [13]. Brucite can be applied to adsorb toxic anionic metals and metalloids, such as arsenic, antimony, and phosphate, because of its positively charged surface layers [14–16]. Therefore, brucite has been broadly used to synthesize hydrotalcite mineral in which there is isomorphic substitution by trivalent metals to the sites of Mg^{2+} in brucite surface layers [16,17]. Some studies have shown that brucite plays a vital role in selectively adsorbing antimonate (Sb(V)) ions on its surfaces [10,11,13]. According to Friedrich et al. [13], antimony can make a brandholzite-like structure through the complexation with magnesium species, which represents that hydrogen bonds interconnect $Mg(H_2O)_6$ and $Sb(OH)_6$ octahedra units. The hydrogen bonding involves the interactions between the hydroxide of brucite and antimonate to form a brandholzite-like structure as a new precipitation form. A few researchers reported that antimony selectively reacts with magnesium to form a hydroxide-containing layered double hydroxide [10,11]. In addition, Lee et al. [12] demonstrated that the desorption of antimony-adsorbed Mg/Al layered double hydroxide requires potent desorption agents due to the secured selective immobilization.

In recent years, industrial wastes have been considered promising material as adsorbents because the reuse of industrial wastes can effectively remove water contaminants and prevent secondary pollution during their disposal and treatment [18]. During the last decades, a variety of iron and aluminum-based wastes, including fly ash, red mud, and acid mine drainage sludge, have been utilized as potential adsorbents, geopolymer, and soil fertilizer due to its massive production [18–20]. In the nuclear power plants, hypochlorous acid produced through on-site electrolysis using seawater is commonly used to prevent biological clogging in the ternary coolant because of its easy production and simple operation [21,22]. During the electrolysis process, seawater is electrochemically decomposed to chlorine (Cl_2) in cathode and sodium hydroxide in the anode. Chlorine molecules react with sodium hydroxide and finally produces hypochlorous acid. The produced hypochlorous acid stored in a storage tank is used to remove biological substances in the intake of seawater in the nuclear power plants. In the storage tank, the mixture of hypochlorous acid and other ionic substances, including chloride, calcium, and magnesium ions, exists as a liquid state and magnesium preferentially forms magnesium hydroxide precipitate due to its low solubility product constant ($K_{sp} = 5.61 \times 10^{-12}$) [23]. Finally, magnesium hydroxide can be settled down in the storage tank as value-added by-products. Although the huge amount of precipitate is periodically generated in the storage tank, this precipitate is abandoned after the drying process. Therefore, research on the removal of metal species using the brucite-rich precipitate (BP) produced from the maintenance of the ternary coolant system in industrial facilities (e.g., nuclear power plants) has been rarely investigated.

This study aims to assess the feasibility of the BP generated in a hypochlorous storage tank in a nuclear power plant as a low-cost adsorbent to immobilize antimony in surface water or wastewater. Thus, the BP was characterized with various analytical techniques and directly correlated to the observed adsorption behaviors, kinetics, and isotherms to better understand the recyclable applicability of the BP to remove antimony in aqueous solutions. Furthermore, the adsorption mechanisms of antimony by the BP through the surface-induced precipitation were also identified with X-ray diffraction spectroscopy.

2. Materials and Methods

2.1. Collection of Brucite-Rich Precipitate (BP)

The BP was collected from the hypochlorous acid storage tank in the nuclear power plant in South Korea during the cleaning period of the storage tank. The collected wet precipitate was washed by deionized (DI) water several times to remove excess impurities on the BP surfaces and then dried at room temperature (20–25 °C) overnight. The dried BP was homogenized by hand grinding and finally sieved through a standard sieve of 0.075 μm opening (200 mesh).

2.2. Characterization of BP

To examine the physicochemical characteristics of the BP, X-ray diffraction patterns were obtained from a high-resolution X-ray diffractometer (XRD, Rigaku, Tokyo, Japan) with Cu Kα radiation and 2θ ratio from 5 to 85°. X-ray fluorescence (XRF, PANalytical Axios, Almelo, The Netherlands) spectroscopy was used to measure the elemental contents of BP quantitatively. The surface images and elemental composition of the BP were obtained by field emission-scanning electron microscope (FE-SEM) with energy dispersive X-ray (EDX) spectroscopy (Hitachi S-4500, Tokyo, Japan). In order to calculate the point of zero charge (PZC), initial pH and equilibrium pH were measured, and the pH_{pzc} was estimated using a plot between ΔpH and equilibrium pH.

2.3. Adsorption Studies

An antimony stock solution was prepared using $KSb(OH)_6$ (concentration of antimony = 1000 mg/L; Sigma Aldrich, St Louis, MO, USA). The bath adsorption experiments for the removal of antimony by the BP were performed using a shaking incubator under controlled conditions (initial antimony concentration = 50 mg/L, BP dose = 0.5 g/L, and temperature = 25 °C). The effects of pH on the adsorption of antimony using the BP were examined by varying solution pH from 3 to 11 by adding 0.1 M HCl and 0.1 M NaOH (Sigma Aldrich, St Louis, MO, USA) solutions. The competitive effects of the co-existing anions on the adsorption of antimony with the BP (initial antimony concentration = 10 mg/L) were determined based on the presence of sulfate, nitrate, bicarbonate, and phosphate ions; each anion solution was respectively prepared using NaCl, Na_2SO_4, $NaNO_3$, $NaHCO_3$, and NaH_2PO_4 (each anion concentration = 10 mg/L; Sigma Aldrich, St Louis, MO, USA). The adsorption kinetic tests were conducted in the reaction time from 10 to 1440 min, and the data were fitted to pseudo-first and second order kinetic models. The adsorption isotherm experiments were carried out under a series of antimony concentrations from 1 mg/L to 150 mg/L. Finally, the data were fitted to the Langmuir and Freundlich Isotherm models. All the samples were filtered using 0.45 μm cellulose acetate membrane filters (Advantec, Tokyo, Japan) to eliminate the suspensions and the antimony concentrations were measured by inductively-coupled plasma mass spectrometry (7700, Agilent, Pal Alto, CA, USA).

3. Results and Discussion

3.1. Mineralogical Characteristics of BP

The mineralogical properties of the BP were characterized by XRF (Table 1). The BP mainly consisted of magnesium (72.5 wt. %) and additionally contained sodium (8.6 wt. %), aluminum (2.5 wt. %), calcium (0.8 wt. %), sulfur (0.8 wt. %), and chlorine (14.7 wt. %). These results are evidence that those elements in seawater could be co-precipitated in the hypochlorous storage tank of the nuclear power plant. Furthermore, magnesium included in the BP exists in the form of magnesium hydroxide due to its relatively low solubility constant ($K_{sp} = 5.61 \times 10^{-12}$) compared to calcium hydroxide ($K_{sp} = 5.5 \times 10^{-6}$) [24]. Figure 1a shows the XRD patterns of the BP. The XRD results of the BP were in good agreement with the typical properties of magnesium hydroxide (brucite). The representative XRD peaks derived from brucite were observed at the reflection of (101), (102), (110), (111), and (201) at the 2θ degree of 38.02 and 50.86, 58.64, 62.07, and 72.03, respectively. In general, the reflection of (001)

at the 2θ degree of 18.8 was intimately related to the needle-shaped magnesium hydroxide. However, there was no peak for (001) in the BP as the heterogeneous precipitate by incorporating other cations, such as sodium, calcium, and aluminum might lead to the formation of magnesium hydroxide with low crystallinity contents [25].

Table 1. Elemental composition of BP.

	Na	Mg	Al	Ca	S	Cl
wt. (%)	8.6	72.5	2.5	0.8	0.8	14.7

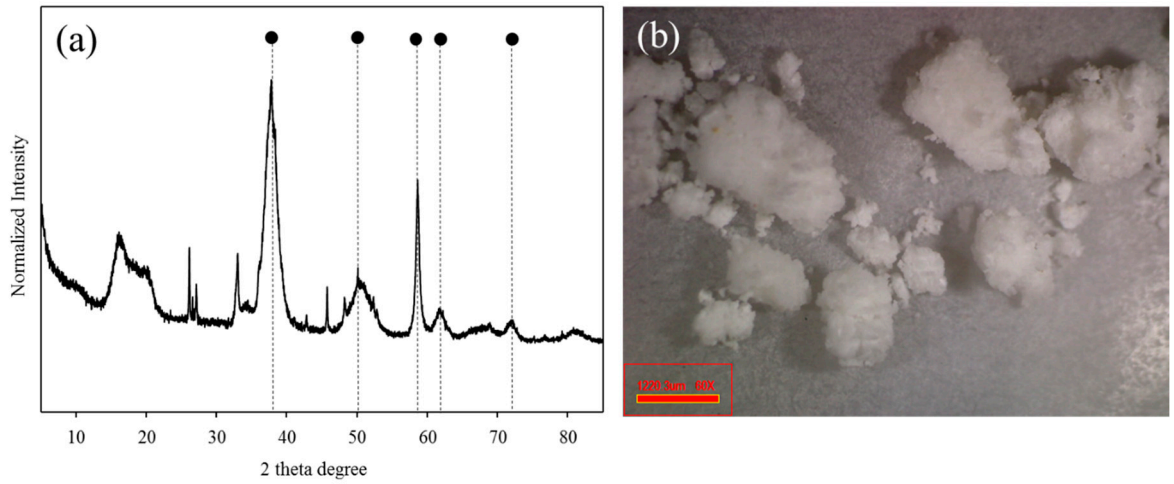

Figure 1. The X-ray diffraction pattern (**a**) and the microscopic image (**b**) of the brucite (magnesium hydroxide)-rich precipitate (BP).

The microscopic image of BP is depicted in Figure 1b. The appearance of BP seemed to be white-colored particles which were consistent with the typical apparent properties of magnesium hydroxide and calcium hydroxide. In order to increase the purity of the precipitate these aggregated particles were crashed and washed by DI water prior to subsequent adsorption experiments. Figure 2 illustrates the FE-SEM image and the EDX spectra of the BP. The BP surfaces exhibited irregular spherical mineral forms and there was no needle-shaped magnesium hydroxide, which was probably due to its low crystallinity [25]. In addition, the EDX results revealed that the BP was predominantly composed of carbon (16.54%), magnesium (17.26%), and oxygen (62.2%). The combined information from the mineralogical characteristics of the BP confirms again that magnesium hydroxide with low crystallinity contents was the dominant component of the BP.

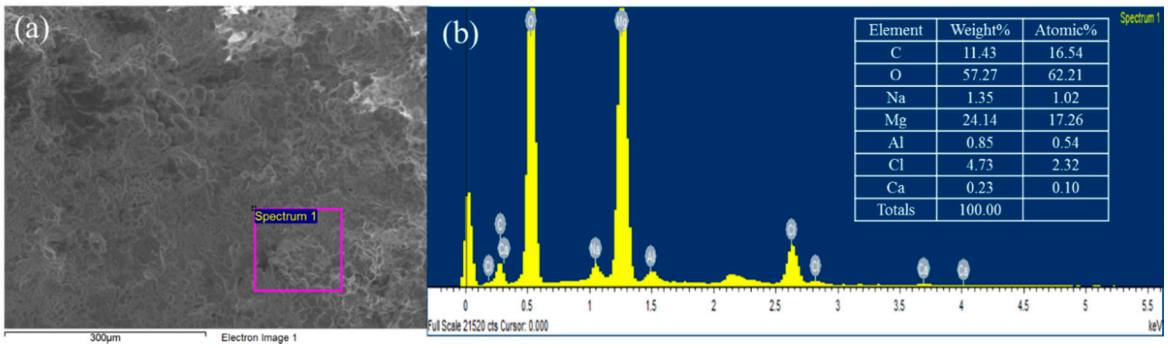

Figure 2. The FE-SEM image (**a**) and the energy dispersive X-ray (EDX) spectra (**b**) of the BP.

Figure 3 shows the point of zero charge (PZC) of the BP in terms of initial and equilibrium pH conditions. The PZC of the BP was slightly lower (pH_{pzc} = 9.6) than that of the typical brucite

reported in the previous study because the BP showed heterogeneous properties due to the irregular co-precipitation process during the hypochlorous acid production through the seawater electrolysis [26]. Therefore, other co-precipitated elements, including calcium, sodium, and aluminium, could change the physical properties of brucite, such as PZC. In general, pH_{pzc} is known to be a critical factor determining the adsorption behavior of charged ions toward charged adsorbents (i.e., electrostatic interactions): (i) equilibrium pH < pH_{pzc} (the surface charge of adsorbents showed a positive surface charge) and (ii) equilibrium pH > pH_{pzc} (the negatively charged adsorbents could effectively remove positively charged contaminants) [12]. Therefore, the PZC should be considered to select the optimum pH for maximizing the removal efficiency of anionic metal species during the adsorption processes. Since the PZC of BP was found at pH 9.6, it is expected that the BP might be practically applicable for the removal of antimony from surface water and/or wastewater because antimony had negative charge properties under neutral pH conditions (i.e., $Sb(OH)_6^-$) [12].

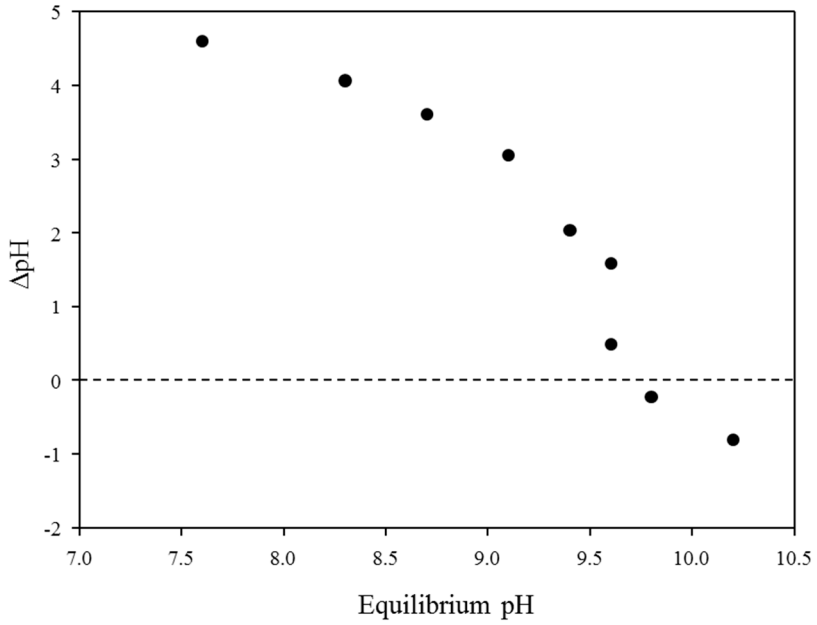

Figure 3. The point of zero charge of BP as a function of initial and equilibrium pH at 25 °C.

3.2. Identification of New Mineral Deposits with Antimony

The XRD spectra of the BP and the antimony adsorbed BP were compared to investigate the new mineral deposits through the electrostatic interactions between the BP and antimony (Figure 4). The XRD patterns of the antimony adsorbed BP were similar to those of the BP. However, the antimony adsorbed BP showed a distinctive XRD peak associated with brandholzite at around 20°. These results imply that a brandholzite-like structure was formed through the complexation of magnesium contents of the BP with antimony [10–13]. The brandholzite-like structure of the antimony adsorbed BP was indicative of $Mg(H_2O)_6$ and $Sb(OH)_6$ octahedra units which were interconnected by hydrogen bonding [13]. These octahedra units were arranged in two types of layers loaded along the c-axis [13]. In the mineral structure, one layer consisted of a single $Sb(OH)_6$ octahedra unit, while the other layer was composed of $Mg(H_2O)_6$ and $Sb(OH)_6$ octahedra units [13]. Our previous research demonstrated that the hydrogen bonding between each octahedral unit by extended X-ray absorption spectroscopy could be mainly attributed to the outer-sphere complex of antimony adsorption by magnesium-rich adsorbents [12]. The remarkable increase in the intensity of the XRD peak related to brandholzite at 20° after the adsorption of antimony (black rhombus) clearly shows that the selective adsorption of antimony using the BP led to the formation of a brandholzite-like structure [12].

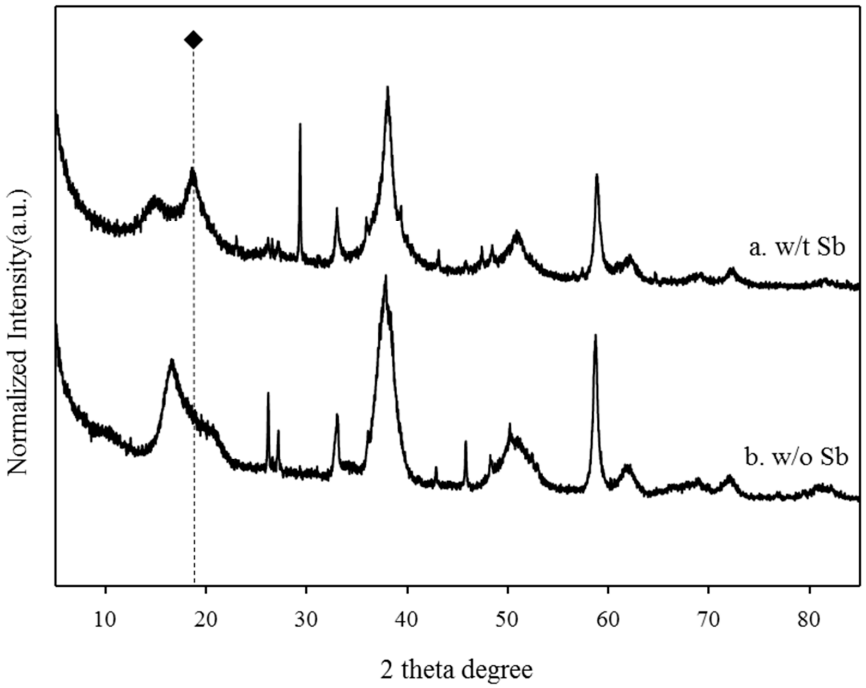

Figure 4. The comparison of XRD patterns of (**a**) antimony adsorbed BP and (**b**) raw BP.

3.3. Adsorption Studies

Figure 5a shows the effects of the solution pH on the adsorption of antimony with the BP. The adsorption of antimony toward the BP varied considerably depending on the solution pH. In the pH range of 3–9, the amount of the adsorbed antimony onto the BP was constantly maintained (adsorption capacity of antimony = 6.63–9.82 mg/g) because of the PZC value of the BP (pH_{pzc} = 9.6), with the exception of pH 3. However, the adsorption efficiency of antimony was gradually decreased when the solution pH was higher than the PZC value of the BP since the electrostatic repulsion between the negatively charged antimony and the negatively charged BP surfaces could interfere with the adsorption of antimony with the BP [12]. Therefore, the lowest adsorption of antimony using the BP was found at pH 11 (adsorption capacity of antimony = 6.63 mg/g). A possible explanation for the slightly lower adsorption of antimony at pH 3 is that the lowered crystallinity of brucite due to the partial dissolution of inorganic materials under acidic conditions could reduce the adsorption efficiency of antimony using the BP [12]. Based on these observations, the neutral pH (pH = 7) was selected as the optimal pH for subsequent adsorption experiments.

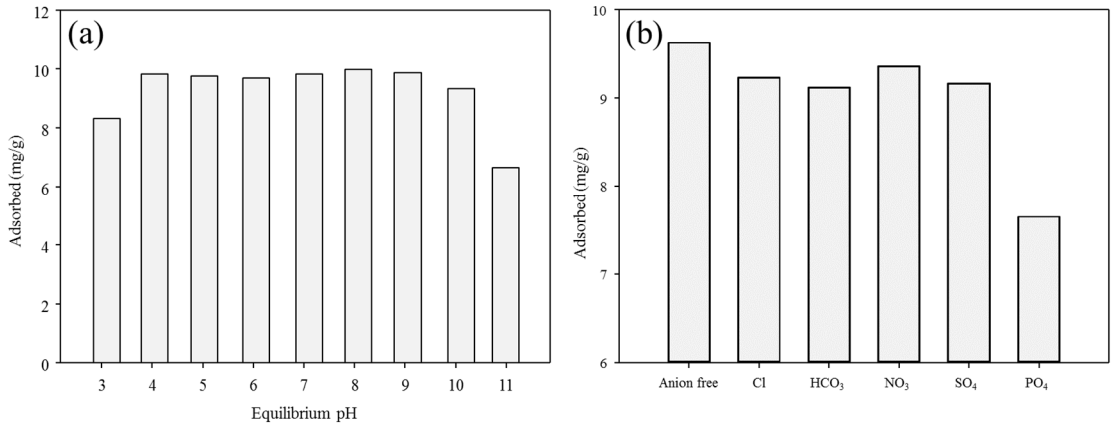

Figure 5. The effects of (**a**) pH and (**b**) co-existing anions (pH = 7, 25 °C) on antimony adsorption by BP.

The effects of co-existing anions on the adsorption of antimony toward the BP were investigated with five different anions as the adsorption efficiency of anionic metals species might be significantly influenced by the sizes of anions, charge density, and the surface charge of adsorbents [27]. As presented in Figure 5b, all the selected anion species (i.e., chloride, bicarbonate, nitrate, sulfate, and phosphate ions) offered negative effects on the adsorption of antimony using the BP. Nevertheless, the degree of hindrance generated from the co-existence of anionic species depended highly according to the differences in their selectivity with antimony [28]. Chloride, bicarbonate, nitrate, and sulfate ions did not considerably inhibit the antimony adsorption using the BP as these anion species had a lower selectivity for antimony ions because of their low charge density [12]. In contrast, a relatively strongly inhibitor effect was found for the adsorption of antimony in the presence of phosphate ions. The higher sorption affinity of phosphate ions toward antimony was likely due to their relatively lower ionic radius (0.17 Å) compared to antimony (ionic radius of Sb(V) = 0.62 Å) which was intimately associated with the surface charge density [12]. These observations indicate that the effects of co-existence anions should be considered for the efficient removal of antimony during the BP-based adsorption processes.

3.4. Kinetic and Isotherm Studies

The time dependence for the removal of antimony by the BP was investigated through the adsorption tests with 50 mg/L of antimony solution at pH 7 (Figure 6a). The obtained data were fitted by the pseudo-first-order and pseudo-second-order kinetic models:

$$\text{Pseudo-first-order kinetic model: } \ln (Q_e - Q_t) = \ln Q_e - k_1 t \quad (1)$$

$$\text{Pseudo-second-order kinetic model: } t/Q_t = 1/(k_2 Q_e^2) + t/Q_e \quad (2)$$

where Q_e (mg/g) is the equilibrium adsorption capacity, Q_t (mg/g) is the adsorption capacity at time t (min), and k_1 (min^{-1}) and k_2 (g min^{-1} mg^{-1}) are rate constants for the pseudo-first-order and pseudo second-order kinetic model, respectively [29].

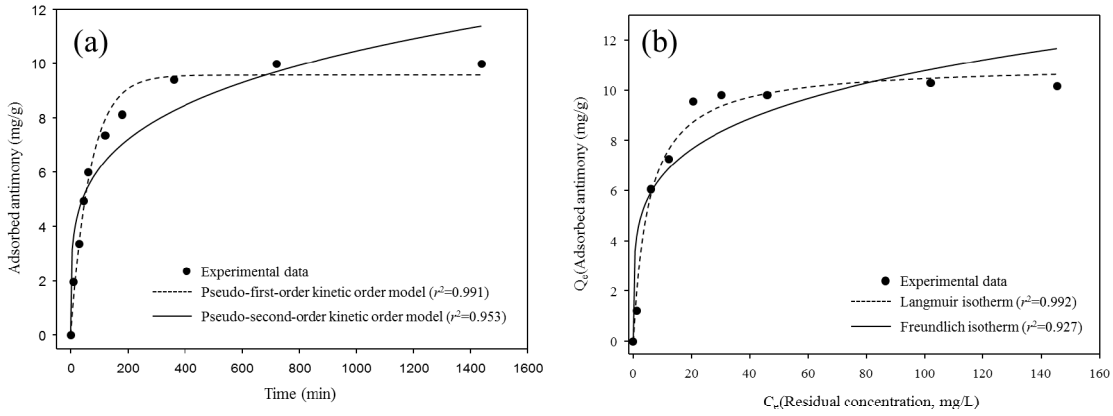

Figure 6. The adsorption kinetics (**a**) and isotherms (**b**) of antimony using BP (25 °C).

The amount of the adsorbed antimony on the BP was rapidly increased in the initial phase (0−300 min) and then its adsorption was equilibrated within 700 min. The kinetic parameters determined from the adsorption of antimony for the BP using the pseudo-first-order and pseudo-second-order kinetic models are provided in Table 2. The adsorption of antimony toward the BP was well-fitted to the pseudo-first-order kinetic model (R^2 = 0.991) rather than the pseudo-second-order kinetic model (R^2 = 0.951). These results suggest that the occupation rates of the adsorption sites were directly proportional to the numbers of the available adsorption sites of the BP surfaces and pores with forming brandholzite-like structure [11,12].

Table 2. The kinetic constants for removal of antimony using BP.

Pseudo-First-Order Kinetic ($\ln(Q_e - Q_t) = \ln Q_e - k_1 t$)			Pseudo-Second-Order Kinetic ($t/Q_t = 1/k_2 Q_e^2 + t/Q_e$)		
Q_e (mg/g)	k_1 (min^{-1})	R^2	Q_e (mg/g)	k_2 (g mg^{-1} min^{-1})	R^2
9.739	9.7×10^{-2}	0.991	7.960	1.4×10^{-1}	0.953

The Langmuir and Freundlich isotherm models were applied to investigate how antimony interacts with the BP as follows:

$$\text{Langmuir isotherm model: } Q_e = K_L\, Q_{max}\, C_e/(1 + K_L\, C_e) \quad (3)$$

$$\text{Freundlich: isotherm model: } Q_e = K_F\, C_e^{1/n} \quad (4)$$

where Q_{max} (mg/g) is the maximal adsorption capacity, and K_L (L/mg) is the Langmuir adsorption constant, n is the site energy heterogeneity factor, and K_F ((mg/g)/(mg/L)n) is the Freundlich constant.

The estimated isotherm models and the isotherm parameters obtained from the adsorption of antimony using the BP are provided in Figure 6b and Table 3, respectively. The adsorption of antimony for the BP was better described by the Langmuir isotherm model (R^2 = 0.992) than the Freundlich isotherm model (R^2 = 0.927). This is the evidence that the monolayer adsorption governed the removal of antimony toward the BP during the adsorption processes [30]. Although the maximum adsorption capacity of the BP antimony calculated using the Langmuir isotherm model (Q_{max} = 11.02 mg/g) was relatively lower than that of the other adsorptive materials (Table 4), the BP might provide several advantages for the practical removal of antimony from surface water and/or wastewater, including massive production, high selectivity, cost effectiveness, and simple preparation [28,31–33]. From these observations, it can be postulated that the use of BP seemed to be a viable way for removing antimony in aqueous solutions and prevent possible secondary contamination during subsequent disposal and treatment procedures.

Table 3. The isotherm constants for removal of antimony by BP.

Langmuir Isotherm ($K_L\, Q_{max}\, C_e/(1 + K_L\, Ce)$)			Freundlich Isothemr ($K_F\, C_e^{1/n}$)		
Q_{max} (mg/g)	K_L (L/mg)	R^2	K_F	n	R^2
11.02	0.187	0.992	4.405	4.708	0.927

Table 4. The maximum adsorption capacity of antimony using BP.

Material	Removal Capacity (mg/g)	pH	Reference
Fe-rich waste	9.13	7.0	[31]
Municipal compost	29.94	4.5	[32]
Tannin	24.0	6.0	[28]
biochar	44.01	5.0	[33]
BP	11.02	7.0	This study

4. Conclusions

In this study, the removal of antimony using the BP collected from the hypochlorous storage tank of the nuclear power plant in aqueous solutions has been investigated to assess its feasibility as a low-cost adsorbent. The BP predominantly consisted of magnesium (72.5%) and its major mineral phase was magnesium hydroxide (brucite). The XRD results revealed that brandholzite-like structures were newly formed on the surfaces of the antimony adsorbed BP. The pH was found to be a dominant factor affecting the adsorption behavior for antimony using the BP due to the pH_{pzc} (9.6). In addition,

the co-existence of anionic species did not significantly affect the adsorption between the BP and antimony due to the selective formation of a brandholzite-like structure. In spite of the lower maximum adsorption capacity (Q_{max} of the BP = 11.02 mg/g) compared with the other adsorptive materials, the BP might offer several benefits (i.e., massive production, high selectivity, cost effectiveness, and simple preparation) for the removal of antimony from surface water and/or wastewater. Therefore, the BP collected from the hypochlorous storage tank of the nuclear power plants was considered to be an effective option for the selective removal of antimony in aqueous solutions due to its brucite-rich nature.

Author Contributions: Conceptualization, S.-H.L. and K.C.; Data curation, K.-H.L. and S.-H.L.; Formal analysis, S.-H.L. and K.-H.L.; Investigation, S.-H.L.; Methodology, S.-H.L. and J.S.; Project administration, K.-H.L.; Resources, Y.-G.L.; Supervision, S.-H.L. and K.C.; Validation, Y.-G.L. and S.-H.L.; Visualization, Y.-G.L. and J.S.; Writing—original draft, K.-H.L.; Writing—review, and editing, S.-H.L. and K.C. All authors have read and agreed to the published version of the manuscript.

Funding: This study was supported by a research project (A17IP05) from Central Research Institute in Korea Hydro & Nuclear Power Co., Ltd.

Conflicts of Interest: The authors declare no conflict of interest.

References

1. Shtangeeva, I.; Bali, R.; Harris, A. Bioavailability and toxicity of antimony. *J. Geochem. Explor.* **2011**, *110*, 40–45. [CrossRef]
2. Sundar, S.; Chakravarty, J. Antimony toxicity. *Int. J. Environ. Res. Public Health* **2010**, *7*, 4267–4277. [CrossRef] [PubMed]
3. Filella, M.; Belzile, N.; Chen, Y.W. Antimony in the environment: A review focused on natural waters I. Occurence. *Earth-Sci. Rev.* **2002**, *57*, 125–176. [CrossRef]
4. US EPA. *Antimony: An Environmental and Health Effects Assessment*; US EPA: Washington, DC, USA, 1984.
5. Lee, S.H.; Choi, H.; Kim, K.W. Removal of As(V) and Sb(V) in water using magnetic nanoparticle-supported layered double hydroxide nanocomposites. *J. Geochem. Explor.* **2018**, *184*, 247–254. [CrossRef]
6. Kolbe, F.; Weiss, H.; Morgenstern, P.; Wennrich, R.; Lorenz, W.; Schurk, K.; Stanjek, H.; Daus, B. Sorption of aqueous antimony and arsenic species onto akaganeite. *J. Colloid Interface Sci.* **2011**, *357*, 460–465. [CrossRef]
7. Lu, H.; Zhu, Z.; Zhang, H.; Zhu, J.; Qiu, Y. Simultaneous removal of arsenate and antimonate in simulated and practical water samples by adsorption onto Zn/Fe layered double hydroxide. *Chem. Eng. J.* **2015**, *276*, 365–375. [CrossRef]
8. Qi, Z.; Lan, H.; Joshi, T.P.; Liu, R.; Liu, H.; Qu, J. Enhanced oxidative and adsorptive capability towards antimony by copper-doping into magnetite magnetic particles. *RSC Adv.* **2016**, *6*, 66990–67001. [CrossRef]
9. Wu, F.; Fu, Z.; Liu, B.; Mo, C.; Chen, B.; Corns, W.; Liao, H. Health risk associated with dietary co-exposure to high levels of antimony and arsenic in the world's largest antimony mine area. *Sci. Total Environ.* **2011**, *409*, 3344–3351. [CrossRef]
10. Kameda, T.; Nakamura, M.; Yoshioka, T. Removal of antimonate ions from an aqueous solution by anion exchange with magnesium-aluminum layered double hydroxide and the formation of a brandholzite-like structure. *J. Environ. Sci. Health. A Tox. Hazard. Subst. Environ. Eng.* **2012**, *47*, 1146–1151. [CrossRef]
11. Kameda, T.; Honda, M.; Yoshioka, T. Removal of antimonate ions and simultaneous formation of a brandholzite-like compound from magnesium-aluminum oxide. *Sep. Purif. Technol.* **2011**, *80*, 235–239. [CrossRef]
12. Lee, S.-H.; Tanaka, M.; Takahashi, Y.; Kim, K.-W. Enhanced adsorption of As(V) and Sb(V) by calcined Mg/Al layered double hydroxide: Investigation of comparative adsorption mechanism by surface characterization. *Chemosphere* **2018**, *211*, 903–911. [CrossRef]
13. Friedrich, A.; Wildner, M.; Tillmanns, E.; Merz, P.L. Crystal chemistry of the new mineral brandholzite, Mg(H2O)6[Sb(OH)6]2, and of the synthetic analogues M2+(H2O)6[Sb(OH)6]2 (M2+ = Mg, Co). *Am. Mineral.* **2000**, *85*, 593–599. [CrossRef]
14. Tanaka, K.; Kozai, N.; Ohnuki, T.; Grambow, B. Study on coordination structure of Re adsorbed on Mg-Al layered double hydroxide using X-ray absorption fine structure. *J. Porous Mater.* **2019**, *26*, 505–511. [CrossRef]

15. Cai, P.; Zheng, H.; Wang, C.; Ma, H.; Hu, J.; Pu, Y.; Liang, P. Competitive adsorption characteristics of fluoride and phosphate on calcined Mg-Al-CO3 layered double hydroxides. *J. Hazard. Mater.* **2012**, *213–214*, 100–108. [CrossRef]
16. Goh, K.H.; Lim, T.T.; Dong, Z. Application of layered double hydroxides for removal of oxyanions: A review. *Water Res.* **2008**, *42*, 1343–1368. [CrossRef] [PubMed]
17. Wang, Q.; Ohare, D. Recent advances in the synthesis and application of layered double hydroxide (LDH) nanosheets. *Chem. Rev.* **2012**, *112*, 4124–4155. [CrossRef]
18. Mohan, D.; Pittman, C.U. Arsenic removal from water/wastewater using adsorbents—A critical review. *J. Hazard. Mater.* **2007**, *142*, 1–53. [CrossRef]
19. Ahmaruzzaman, M. Industrial wastes as low-cost potential adsorbents for the treatment of wastewater laden with heavy metals. *Adv. Colloid Interface Sci.* **2011**, *166*, 36–59. [CrossRef]
20. Wang, Y.R.; Tsang, D.C.W.; Olds, W.E.; Weber, P.A. Utilizing acid mine drainage sludge and coal fly ash for phosphate removal from dairy wastewater. *Environ. Technol.* **2013**, *34*, 3177–3182. [CrossRef]
21. Chen, S.; Zhu, J.; Wang, B.; Liu, H.; He, B. Experimental study on hypochlorous acid blocking the marine diatom adhesion. *Int. J. Electrochem. Sci.* **2012**, *7*, 5331–5338.
22. Sandvik, E.L.; McLeod, B.R.; Parker, A.E.; Stewart, P.S. Direct electric current treatment under physiologic saline conditions kills staphylococcus epidermidis biofilms via electrolytic generation of hypochlorous acid. *PLoS ONE* **2013**, *8*, e55118. [CrossRef] [PubMed]
23. Schwartz, A.M. Solutions and solution properties. In *Handbook of Industrial Crystallization*; Elsevier: Amsterdam, The Netherlands, 2002; Volume 7, Chapter 1; pp. 1–31. [CrossRef]
24. Zheng, L.; Xuehua, C.; Mingshu, T. Hydration and setting time of MgO-type expansive cement. *Cem. Concr. Res.* **1992**, *22*, 1–5. [CrossRef]
25. Wang, X.; Pang, H.; Chen, W.; Lin, Y.; Ning, G. Controllable fabrication of high purity $Mg(OH)_2$ nanoneedles via direct transformation of natural brucite. *Mater. Lett.* **2014**, *120*, 69–72. [CrossRef]
26. Pokrovsky, O.S.; Schott, J. Experimental study of brucite dissolution and precipitation in aqueous solutions: Surface speciation and chemical affinity control. *Geochim. Cosmochim. Acta* **2004**, *68*, 31–45. [CrossRef]
27. Lee, S.-H.; Kim, K.-W.; Lee, B.-T.; Bang, S.; Kim, H.; Kang, H.; Jang, A. Enhanced arsenate removal performance in aqueous solution by yttrium-based adsorbents. *Int. J. Environ. Res. Public Health* **2015**, *12*, 13523–13541. [CrossRef] [PubMed]
28. Bacelo, H.; Vieira, B.R.C.; Santos, S.C.R.; Boaventura, R.A.R.; Botelho, C.M.S. Recovery and valorization of tannins from a forest waste as an adsorbent for antimony uptake. *J. Clean. Prod.* **2018**, *198*, 1324–1335. [CrossRef]
29. Yu, Y.; Yu, L.; Wang, C.; Chen, J.P. An innovative yttrium nanoparticles/PVA modified PSF membrane aiming at decontamination of arsenate. *J. Colloid Interface Sci.* **2018**, *530*, 658–666. [CrossRef]
30. Tang, M.; Chen, J.; Wang, P.; Wang, C.; Ao, Y. Highly efficient adsorption of uranium(VI) from aqueous solution by a novel adsorbent: Titanium phosphate nanotube. *Environ. Sci. Nano* **2018**. [CrossRef]
31. Lee, S.-H.; Takahashi, Y. Carbothermal preparation of magnetic-responsible ferrihydrite based on Fe-rich precipitates for immobilization of arsenate and antimonate: Batch and spectroscopic studies. *Chemosphere* **2019**, *237*, 124489. [CrossRef]
32. Diquattro, S.; Garau, G.; Lauro, G.P.; Silvetti, M.; Deiana, S.; Castaldi, P. Municipal solid waste compost as a novel sorbent for antimony(V): Adsorption and release trials at acidic pH. *Environ. Sci. Pollut. Res.* **2018**, *25*, 5603–5615. [CrossRef]
33. Mayakaduwa, S.S.; Kumarathilaka, P.; Herath, I.; Ahmad, M.; Al-Wabel, M.; Ok, Y.S.; Usman, A.; Abduljabbar, A.; Vithanage, M. Equilibrium and kinetic mechanisms of woody biochar on aqueous glyphosate removal. *Chemosphere* **2016**, *144*, 2516–2521. [CrossRef] [PubMed]